Direct imaging of photonic nanojets

Patrick Ferrand,[1] **Jérôme Wenger,**[1] **Alexis Devilez,**[2] **Martina Pianta,**[1] **Brian Stout,**[2] **Nicolas Bonod,**[2] **Evgueni Popov,**[2] **and Hervé Rigneault**[1]

[1] *Institut Fresnel, MOSAIC group, Aix-Marseille Université, CNRS Domaine Universitaire de St Jérôme, 13397 Marseille, France*

[2] *Institut Fresnel, CLARTE group, Aix-Marseille Université, CNRS Domaine Universitaire de St Jérôme, 13397 Marseille, France*

patrick.ferrand@fresnel.fr

www.fresnel.fr/mosaic

Abstract: We report the direct experimental observation of photonic nanojets created by single latex microspheres illuminated by a plane wave at a wavelength of 520 nm. Measurements are performed with a fast scanning confocal microscope in detection mode, where the detection pinhole defines a diffraction-limited observation volume that is scanned in three dimensions over the microsphere vicinity. From the collected stack of images, we reconstruct the full 3 dimensional photonic nanojet beam. Observations are conducted for polystyrene spheres of 1, 3 and 5 μm diameter deposited on a glass substrate, the upper medium being air or water. Experimental results are compared to calculations performed using the Mie theory. We measure nanojet sizes as small as 270 nm FWHM for a 3 μm sphere at a wavelength λ of 520 nm. The beam keeps a subwavelength FWHM over a propagation distance of more than 3 λ, displaying all the specificities of a photonic nanojet.

OCIS codes: (180.0180) Microscopy; (230.3990) Micro-optical devices; (290.4020) Mie theory; (260.2110) Electromagnetic optics

References and links

1. Z. Chen, A. Taflove, and V. Backman, "Photonic nanojet enhancement of backscattering of light by nanoparticles: a potential novel visible-light ultramicroscopy technique," Opt. Express **12**, 1214-1220 (2004).
2. X. Li, Z. Chen, A. Taflove, and V. Backman, "Optical analysis of nanoparticles via enhanced backscattering facilitated by 3-D photonic nanojets," Opt. Express **13**, 526-533 (2005).
3. S. Lecler, Y. Takakura, and P. Meyrueis, "Properties of a 3D photonic jet," Opt. Lett. **30**, 2641-2643 (2005).
4. A. V. Itagi and W. A. Challener, "Optics of photonic nanojets," J. Opt. Soc. Am. A **22**, 2847-2858 (2005).
5. A. Heifetz, J. J. Simpson, S.-C. Kong, A. Taflove, and V. Backman, "Subdiffraction optical resolution of a gold nanosphere located within the nanojet of a Mie-resonant dielectric microsphere," Opt. Express **15**, 17334-17342 (2007).
6. A. Heifetz, K. Huang, A. V. Sahakian, X. Li, A. Taflove, V. Backman, "Experimental confirmation of backscattering enhancement induced by a photonic jet," Appl. Phys. Lett. **89**, 221118 (2006).
7. M. Gerlach, Y. P. Rakovich and J. F. Donegan, "Nanojets and directional emission in symmetric photonic molecules," Opt. Express **15**, 17343-17350 (2007).
8. M. Mosbacher, H.-J. Münzer, J. Zimmermann, J. Solis, J. Boneberg, P. Leiderer, "Optical field enhancement effects in laser-assisted particle removal," Appl. Phys. A: Mater. Sci. Process. **72**, 41-44 (2001).
9. K. Piglmayer, R. Denk, and D. Bäuerle, "Laser-induced surface patterning by means of microspheres," Appl. Phys. Lett. **80**, 4693-4695 (2002).
10. B. S. Luk'yanchuk, N. Arnold, S. M. Huang, Z. B. Wang, and M. H. Hong, "Three-dimensional effects in dry laser cleaning," Appl. Phys. A: Mater. Sci. Process. **77**, 209-215 (2003).

#91087 - $15.00 USD Received 20 Dec 2007; revised 31 Jan 2008; accepted 31 Jan 2008; published 1 May 2008

11. B. S. Luk'yanchuk, Z. B. Wang, W. D. Song, and M. H. Hong, "Particle on surface: 3D-effects in dry laser cleaning," Appl. Phys. A: Mater. Sci. Process. **79**, 747-751 (2004).
12. Y. Zhou, M.H. Hong, J.Y.H. Fuh, L. Lu, B.S. Luk'yanchuk, Z.B. Wang, L. P. Shi, and T. C. Chong, "Direct femtosecond laser nanopatterning of glass substrate by particle-assisted near-field enhancement," Appl. Phys. Lett. **88**, 023110 (2006).
13. Y. Zhou, M.H. Hong, J.Y.H. Fuh, L. Lu, B.S. Luk'yanchuk, Z.B. Wang, "Near-field enhanced femtosecond laser nano-drilling of glass substrate," J. Alloys Compd. **449**, 246-249 (2008).
14. S. Lecler, S. Haacke, N. Lecong, O. Crégut, J.-L. Rehspringer, C. Hirlimann, "Photonic jet driven non-linear optics: example of two-photon fluorescence enhancement by dielectric microspheres," Opt. Express **15**, 4935-4942(2007).
15. Note that the laser source of our LSCM system was not used in the present work. Literally speaking, the term "confocal" is not appropriate here due to the wide field excitation used. See for instance *Confocal and Two-Photon Microscopy: Foundations, Applications and Advances*, A. Diaspro (Ed.), (Wiley-Liss, New York, 2002).
16. J. Enderlein, C. Zander, "Theoretical Foundations of Single Molecule Detection in Solution," in *Single molecule detection in solution*, C. Zander, J. Enderlein, R. A. Keller (Eds.), (Wiley-VCH, Berlin, Germany), pp. 21-67.
17. W. S. Rasband, "ImageJ," U. S. National Institutes of Health, Bethesda, Maryland, USA (1997-2007), http://rsb.info.nih.gov/ij/.
18. R. P. Dougherty, OptiNav, Inc., "Iterative Deconvolve 3D plugin for ImageJ," http://www.optinav.com/imagej.html, accessed Dec. 8, 2007.
19. K. U. Barthel, FHTW Berlin, "Volume Viewer plugin for ImageJ," http://rsb.info.nih.gov/ij/plugins/volume-viewer.html, accessed Dec. 8, 2007.
20. M. I. Mishchenko, L. D. Travis, A. A. Lacis, *Scattering, Absorption, and Emission of Light by Small Particles* (Cambridge University Press , Cambridge, UK, 2002).
21. B. Stout, J. C. Auger, J. Lafait, "Individual and aggregate scattering matrices and cross sections: conservation laws and reciprocity," J. Mod. Opt. , **48**, 2105-2128 (2001).
22. B. Stout, C. Andraud, S. Stout, J. Lafait, "Absorption in multiple scattering systems of coated spheres," J. Opt. Soc. Am. A , **20**, 1050-1059 (2003).
23. B. Stout, M. Nevière, E. Popov, "Light diffraction by a three-dimensional object: differential theory," J. Opt. Soc. Am. A , **22**, 2385-2404(2005).

1. Introduction

Several recent papers have theoretically and numerically investigated the electromagnetic field distribution in the vicinity of a dielectric sphere of micrometer dimensions illuminated by a plane wave [1, 2, 3, 4, 5]. Under certain conditions, these studies predict the existence of a subwavelength-waist beam that emerges from the microsphere with high intensity and low divergence. For instance, for a dielectric sphere (refractive index 1.59) of 3.5 μm diameter operated in air at $\lambda = 400$ nm, a tight full width at half maximum (FWHM) of 190 nm is created at the best focus, the intensity is concentrated up to 160 times, and the beam keeps a subwavelength FWHM over a propagation distance greater than 2.5 λ [2]. These specific features – subwavelength FWHM and micron propagation distance – are unreachable with a classical Gaussian laser beam focused by a high numerical aperture objective. This beam has therefore been termed photonic nanojet [1].

Photonic nanojets form a widely studied subject. However, to the best of our knowledge, only indirect observations of nanojets have been reported so far [6, 7]. Most studies investigated the use of colloidal dielectric microspheres for dry laser cleaning and optical nanolithography applications [8, 9, 10, 11, 12, 13]. Due to the focusing of the incoming laser light in the microsphere near-field, 200-300 nm holes were created in a glass substrate when 1 μm silica beads deposited on glass were illuminated with a femtosecond laser beam [12, 13]. Microspheres were also used to enhance scattering and fluorescence of emitters located in the photonic jet region. Position-dependent backscattering enhancement induced by a photonic jet has been measured experimentally at microwave frequencies [6]. In the optical domain, floating dielectric microspheres have been added to a solution of rhodamine B dyes to enhance the two-photon fluorescence up to 30% thanks to the focusing of the excitation laser beam [14].

In this study, we report the direct experimental observation of photonic nanojets created

#91087 - $15.00 USD Received 20 Dec 2007; revised 31 Jan 2008; accepted 31 Jan 2008; published 1 May 2008

by single latex microspheres of 5, 3 and 1 μm in diameter deposited on a glass coverslip. The measurements were carried out on a fast scanning confocal microscope with the laser excitation being turned off and replaced by a large area collimated beam [15] (See Fig. 1). The confocal detection pinhole defines a 3D observation volume corresponding to the collection efficiency function (CEF) of our microscope setup. Light intensity emerging from the confocal region is recorded as the detection volume is scanned in three dimensions to monitor the propagation of the photonic jet in the microsphere vicinity. From the collected stack of images, we reconstruct the full photonic nanojet beam and discuss its specificities.

The paper is outlined as follows : first, we detail our experimental apparatus and the numerical methods used for the simulations (Section 2). We then present (Section 3) and discuss (Section 4) our results.

2. Materials and methods

2.1. Microspheres

Latex microspheres (refractive index 1.6) of diameter 1, 3 and 5 μm (dispersion below 0.1%) were taken as purchased from Fluka Chemie GmbH (Buchs, Switzerland), diluted in pure water and dispersed on a cleaned microscope coverslip (borosilicate glass, refractive index 1.51, thickness 150 μm) before air drying. Concentration was set so as to reach an average surface density of 1 bead per 30x30 μm^2. Scattering between adjacent microspheres is thus completely avoided.

2.2. Experimental setup

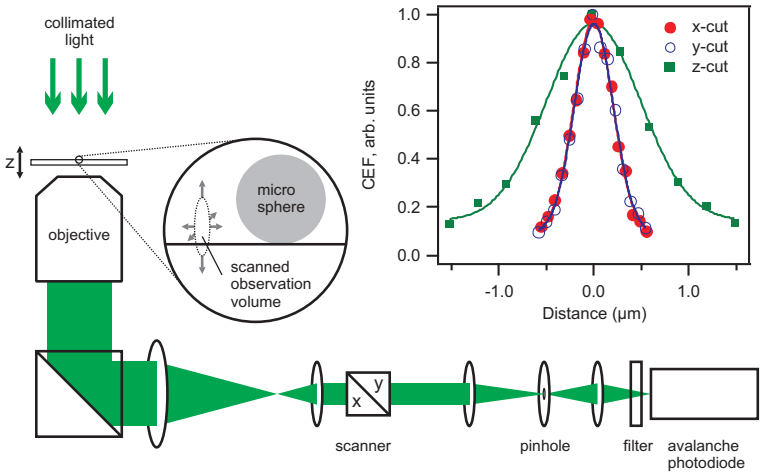

Fig. 1. Schematic of the observation setup (not to scale). The observation volume can be scanned in 3D by acting on both scanner and focus. Inset: Measured CEF for the system.

The measurements were carried out on an Axiovert 200M inverted microscope stand (Carl Zeiss, Jena, Germany), equipped with a custom system of laser scanning confocal microscopy (LSCM). Collimated unpolarized white light was sent to the sample through the microscope condenser set in Köhler illumination with minimum aperture diaphragm opening. Light collection was performed by the LSCM system, as illustrated in Fig. 1. The focal plane of a water immersion C-Apochromat 40x (NA=1.2) objective was imaged with a magnification of 120 on a 75-μm diameter pinhole. The resulting rejection of out-of-plane and out-of-axis light defines

#91087 - $15.00 USD Received 20 Dec 2007; revised 31 Jan 2008; accepted 31 Jan 2008; published 1 May 2008

in the sample a 3D observation volume that can be moved (i) transversely by acting on a set of two galvanometers [model 6200H with dual-axis 673 controller (Cambridge Technology, Cambridge, MA), driven by a PCI-6731 high-speed analog output voltage card (National Instruments, Austin, TX)], (ii) in the axial direction by changing the motorized microscope focus. Detection of light was performed by an avalanche photodiode (SPCM-AQR-14, Perkin Elmer, Fremont, CA) working in a photon counting mode, placed behind a 500–540 nm bandpass filter (XF3080-510AF23, Omega Optical, Brattleboro, VT), in order create quasi monochromatic measurement conditions. A PCI-6602 counter (National Instruments) was used for photocounts acquisition. Scanning (both in plane and in depth) and data acquisition were synchronized and controlled by a graphic user interface developed in house in a LabVIEW environment (National Instruments). The factor for converting the scanning command voltages into real distances in the sample was calibrated using reference samples. Unless specified, data shown in this paper were recorded as stacks of 41 frames (500 nm steps of focus) of 100×100 pixels, with a pixel dwell time of 1 ms. Complete automated acquisition of the whole stack thus took about 400 s.

The observation volume of our system was quantitatively characterized by recording the emission of an isolated 20-nm diameter fluorescent sphere (FluoSpheres F8845 Yellow/green, Molecular Probes, Eugene, OR). For this measurement, we used the epi-fluorescence system with an appropriate reflector cube (38-HE-eGFP, Carl Zeiss) for the wide field excitation. Since the size of the sphere is much smaller than the wavelength in use, it behaves in the far field like a point source, so that the measured intensity for a 3D scan gives directly the detection point spread function of our system, that corresponds to the collection efficiency function (CEF) [16]. A plot of the CEF along the three axis is reported in the inset of Fig. 1, as well as fit by a 3D Gaussian distribution, giving 425 nm and 1120 nm as the transverse and longitudinal FWHMs.

2.3. Data processing

Raw data of photon counts were imported as scaled image stacks and displayed using the public domain program ImageJ [17]. Data were then deconvolved by a 3D Gaussian CEF of same width as the one measured on our system using an iterative 3D deconvolution algorithm [18] and reconstructed in volume by trilinear interpolation [19].

2.4. Numerical methods

Although we aim at investigating the local electromagnetic field produced by the scattering of a homogeneous dielectric sphere, the fact that the spheres studied were all several wavelengths in diameter allows us to work in the context of general Mie theory [20]. Numerical simulations have thus been performed using the quasi-exact Mie theory [21, 22] with analytic expressions for the incident, scattered, and internal fields on a basis of multipolar wave functions **M** and **N** [23]. This approach permits a ready calculation of the field at any point in space to arbitrary accuracy.

The experimental characterization of photonic jets discussed here was performed on a glass substrate. However, the simulations considered only a free-standing microsphere embedded in a homogeneous medium. Although the presence of a substrate plays a role on the formation of the photonic jet, the form of the photonic jet studied here will appear quite similar, quantitatively and qualitatively, to our simulations for the case of a homogeneous medium (see discussion in section 4).

3. Results

Photonic jets have been characterized in the 500-540 nm range for single spheres of diameter 5, 3 and 1 μm, deposited on a glass coverslip. In this section, we present for each diameter the raw data, as well as a reconstructed map of intensity along the axial direction, which has been

#91087 - $15.00 USD Received 20 Dec 2007; revised 31 Jan 2008; accepted 31 Jan 2008; published 1 May 2008

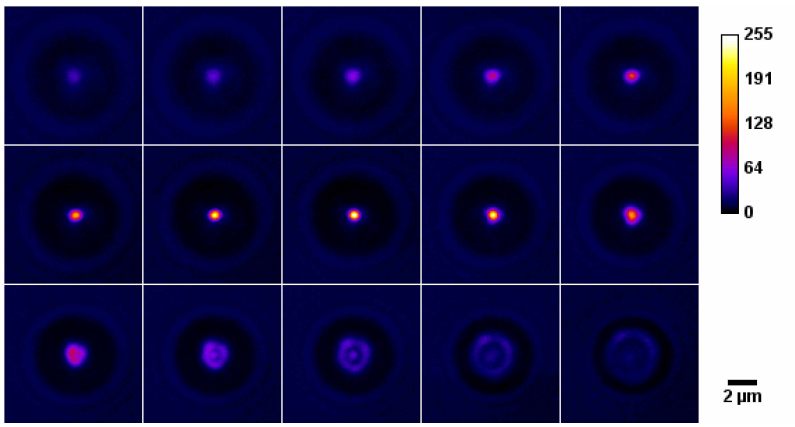

Fig. 2. Raw stack of images taken for a 5 μm sphere illuminated at $\lambda = 520$ nm. The microsphere is deposited on a glass substrate, the upper medium is air. The detection plane moves upwards (towards the bead) by steps of 500 nm between each 2D scan.

corrected for the CEF of our apparatus. Different cuts have been performed on this data to study the profile of the jet and compare it to numerical simulations.

Stack of raw images measured on a 5 μm sphere are shown in Fig. 2. Successive 2D scans correspond to successive imaging planes moving upwards (towards the bead) by steps of 500 nm. The full data set was made of 41 frames. Although the complete stack was processed in this study, only 15 of them recorded around the plane of best focusing are shown in this figure for a better clarity. Data show a local enhancement of intensity for a couple of planes, while concentric rings appear for the other planes. Note that the surrounding area remains at a constant intensity, that will serve later as a reference for quantifying the local intensity enhancement.

Prior to quantitative analysis, the raw data have been corrected by 3D numerical deconvolution, in order to take into account the effects of the CEF of our apparatus, allowing to reconstruct the 3D distribution of light intensity (see section 2.3 for details). A slice along the optical axis, as illustrated in Fig. 3 (a), exhibits clearly the expected focusing effect. The transverse intensity distribution cut along the horizontal axis at the best focus is displayed on Fig. 3 (b), together with a Gaussian fit. Our data bears a remarkable Gaussian lineshape, as expected from theoretical computations [2, 3, 4].

We used the following procedure to estimate the transverse FWHM of the beam at best focus. Starting from the raw stack of images, the plane of best focus was selected. A transverse cut was plotted and fitted by a Gaussian distribution. From the measured FWHM denoted Δ_{raw}, the nanojet FWHM Δ_{jet} was obtained by exploiting the properties of deconvolution of Gaussian functions, so that it is simply given by $\Delta_{\text{jet}} = (\Delta^2_{\text{raw}} - \Delta^2_{\text{CEF}})^{1/2}$, where Δ_{CEF} is the measured FWHM of the CEF of our system, shown on Fig. 1. This procedure turned out to be more accurate and robust than dealing with the numerically deconvolved data [18], since the 3 dimensional deconvolution process is affected by different sources of noise. For the 5 μm sphere, we thus measured a FWHM at best focus of 320 nm, which is below the wavelength taken in the glass medium (520/1.5 = 347 nm).

The local intensity enhancement in the jet was emphasized by plotting the intensity profile along the jet axis, as shown in Fig. 3 (c). Note that the intensity has been normalized so that the incident intensity (measured in the homogeneous surrounding area) was set to unity. For the 5 μm sphere at best focus, we measured a local intensity enhancement of 59. This figure comes

#91087 - $15.00 USD Received 20 Dec 2007; revised 31 Jan 2008; accepted 31 Jan 2008; published 1 May 2008

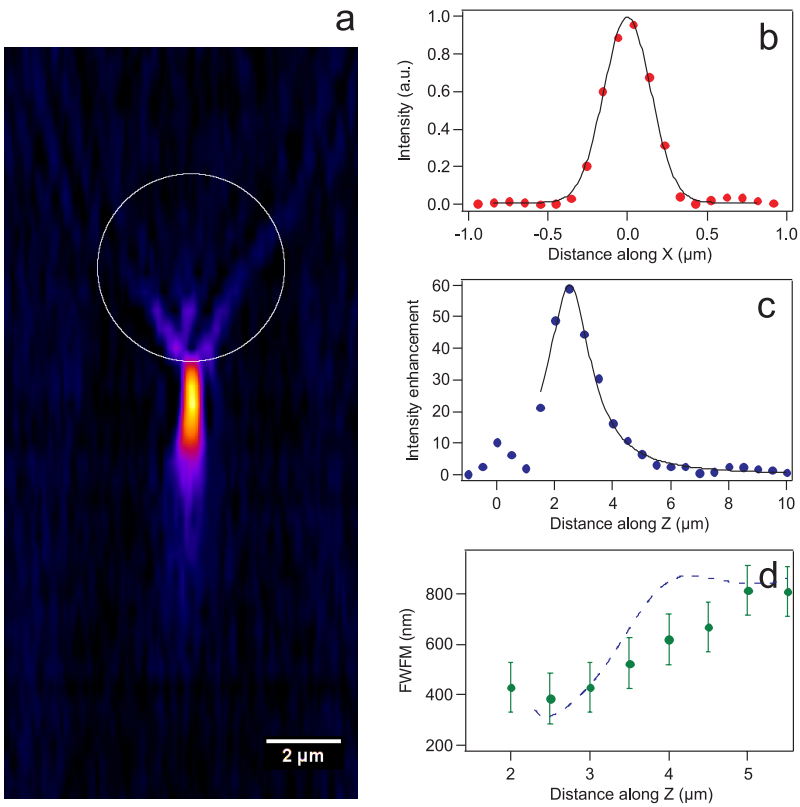

Fig. 3. (a) Reconstruction of the photonic jet generated by a 5 μm microsphere viewed along the optical axis. This refers to the stack of raw data displayed on Fig. 2. The effects of the CEF of our apparatus have been corrected here by numerical deconvolution (see text for details). The microsphere position is indicated by a white circle. (b) Cut along the horizontal axis at the best focus point. Red dots correspond to the measured data after CEF deconvolution, solid line is a Gaussian fit that emphasizes the Gaussian lineshape of the profile. (c) Intensity cut along the vertical axis at the center of the jet. Blue dots correspond to the measured data after CEF deconvolution. Solid line is a Lorenzian fit. The intensity has been normalized so that the incoming intensity (calibrated well outside the bead vicinity) is set to unity. Therefore, this cut directly shows the intensity concentration (enhancement) inside the photonic jet. (d) Full width at half maximum (FWHM) of the photonic jet measured for each 2D scan after CEF deconvolution (green dots). The dashed line corresponds to the FWHM of our numerical simulation for a 5 μm latex bead free standing in air.

close to the surface ratio of the microsphere and nanojet at best focus $\left(\frac{5}{2*0.32}\right)^2 \approx 61$, if we consider two times the FWHM as an approximation for the nanojet total diameter. Moreover, the intensity decay in the jet can be correctly fitted by a Lorentzian lineshape (solid line).

Finally, the jet divergence was assessed by measuring the FWHM of the jet on the deconvolved data for each scanning plane. The obtained values are reported in Fig. 3 (d). It appears that the beam keeps a subwavelength FWHM over a propagation distance of about 1.5 μm. Numerical simulation are reported on the same graph by a dashed line. Possible reasons for which the agreement is only partial will be discussed in section 4.

#91087 - $15.00 USD Received 20 Dec 2007; revised 31 Jan 2008; accepted 31 Jan 2008; published 1 May 2008

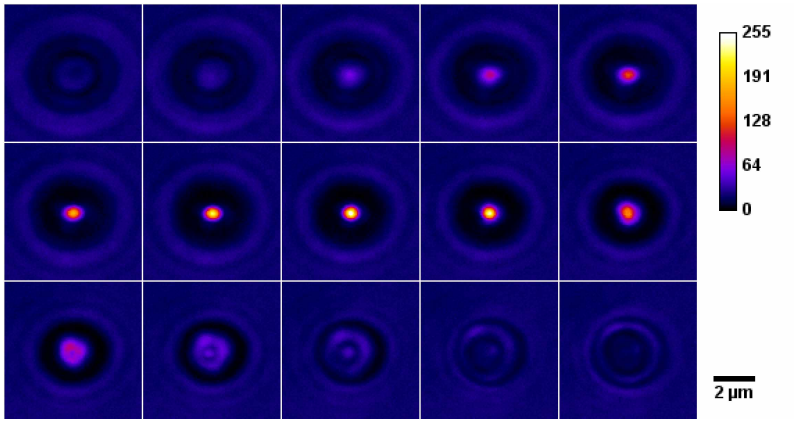

Fig. 4. Same as Fig. 2 for a sphere of 3 μm diameter.

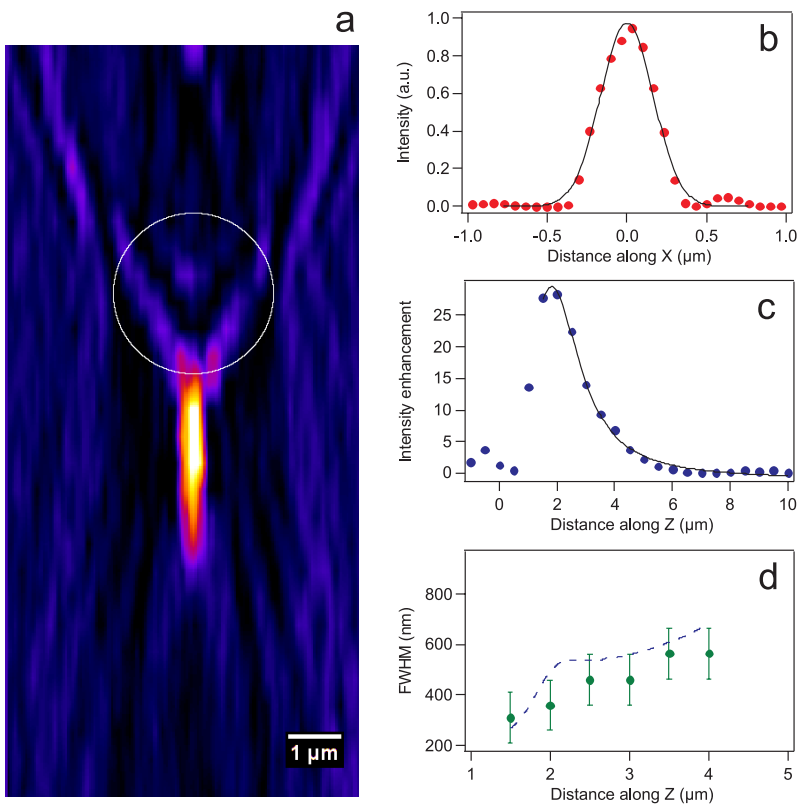

Fig. 5. Same as Fig. 3 for a sphere of 3 μm diameter.

#91087 - $15.00 USD Received 20 Dec 2007; revised 31 Jan 2008; accepted 31 Jan 2008; published 1 May 2008

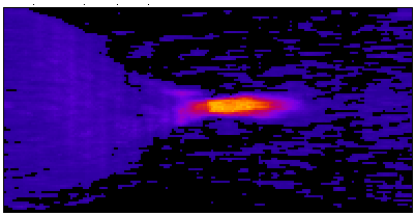

Fig. 6. (1520 KB) Movie of the reconstructed photonic jet for a 3 μm sphere.

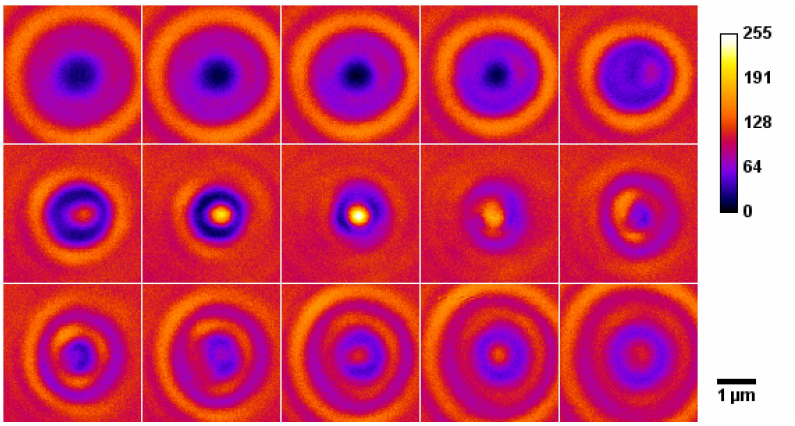

Fig. 7. Same as Fig. 2 for a sphere of 1 μm diameter.

Raw data of the photonic jet measured on a 3 μm are represented in Fig. 4 in the same fashion as in Fig. 2. The same data treatment as previously has been carried out on the data and the results are summarized in Fig. 5. A movie of the photonic jet is presented on Fig. 6. Compared to the previous 5 μm case, the transverse FWHM at best focus is 15% narrower, as we find $\Delta_{\text{jet}} \simeq 270$ nm. The intensity enhancement at the best focus is clearly weaker (we get 29 instead of 59), but this comes with the reduction of the microsphere diameter. Again, the measured intensity enhancement corresponds to the surface ratio of the microsphere and nanojet at best focus $\left(\frac{3}{2*0.27}\right)^2 \approx 31$.

Unlike with larger diameters, the 1 μm sphere shows a weak focusing effect. In raw data of Fig. 7 the intensity in the jet is only twice the incident intensity. The intensity distribution along the propagation axis is mapped in Fig. 8 (a) and 8 (c) after numerical correction for the observation volume. A transverse cut is presented in Fig. 8 (b). It clearly shows the shadowing effect introduced by the microsphere as compared to regions unaffected by the bead. The FWHM of the central spot region can be estimated to about 300 nm. Due to the low contrast of Fig. 8 (a), it was not possible to reliably measure the evolution of the FWHM versus the propagation distance.

The formation of photonic nanojet has been numerically simulated using the Mie theory (see section 2.4) for the spheres of diameters 5 and 3 μm. To simplify the numerical computations, we considered for simulation a free-standing microsphere of index $n = 1.6$ embedded in a homogeneous medium of index unity. Although we are aware that the presence of a substrate may play a role on the formation of the photonic jet, intensity distributions obtained by simulation, and displayed in Fig. 9 are in good agreement with measurements presented in Figs. 3 (a) and 5 (a).

#91087 - $15.00 USD Received 20 Dec 2007; revised 31 Jan 2008; accepted 31 Jan 2008; published 1 May 2008

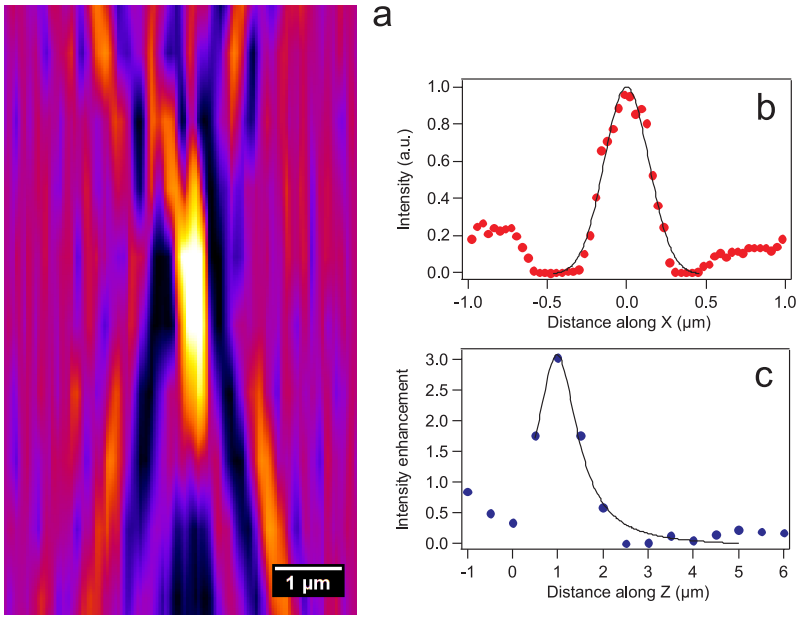

Fig. 8. Same as Fig. 3 for a sphere of 1 μm diameter.

4. Discussion

In order to study the effect of the index contrast between the sphere and the surrounding medium, we have also performed measurements on microspheres deposited on glass and immersed in water ($n = 1.33$). Values of FWHM and intensity enhancement obtained for different sphere diameters are summarized in Tab. 1. They stand in good agreement with the tendency already observed in previous theoretical works [2, 3, 4], as the reduced index contrast gives rise to weaker focusing.

Table 1. Summary of nanojet FWHM and intensity enhancement values measured for different spheres diameters and different refractive indices of the upper medium.

Diameter	FWHM (nm)		Intensity enhancement	
(μm)	air	water	air	water
5.0	320	460	59	42
3.0	270	350	29	22
1.0	300	370	3.0	3.4

Concerning the glass substrate, the comparison between experiments, performed with a glass substrate, and the simulations, performed in a homogeneous medium, shows that the results are qualitatively compatible. It is important here to keep in mind that the nanojets measured experimentally in this work were actually located in the glass. As long as transverse properties are concerned, it is reasonable in a first approximation to consider that the glass substrate introduces no symmetry breakdown, so that these properties (e.g., FWHM) should mostly remain unaffected. However, these considerations do not apply to axial parameters such as the jet divergence. This could explain the relative disagreement observed especially for the 5 μm case (Fig. 3 (d)), and points out the need for more accurate simulations.

Finally, photonic nanojets have been investigated for groups of spheres in contact, which

#91087 - $15.00 USD Received 20 Dec 2007; revised 31 Jan 2008; accepted 31 Jan 2008; published 1 May 2008

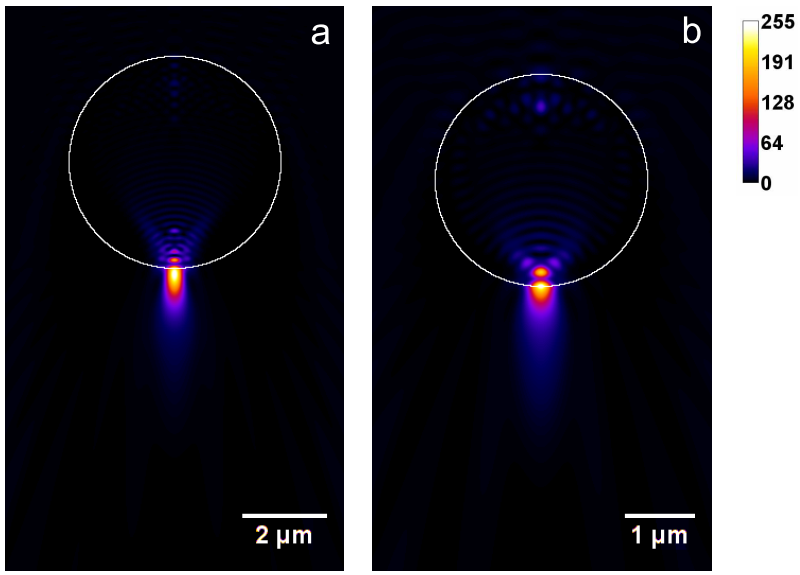

Fig. 9. Distribution of intensity obtained by numerical simulations. (a) Case of a 5 μm sphere. Dependance of FWHM of the jet versus propagation distance was plotted in Fig. 3 (d). (b) Case of a 3 μm sphere. Dependance of FWHM of the jet versus propagation distance was plotted in Fig. 5 (d). For both figures, the corresponding sphere location and size are indicated by a white circle. Note that the color levels have been normalized independently.

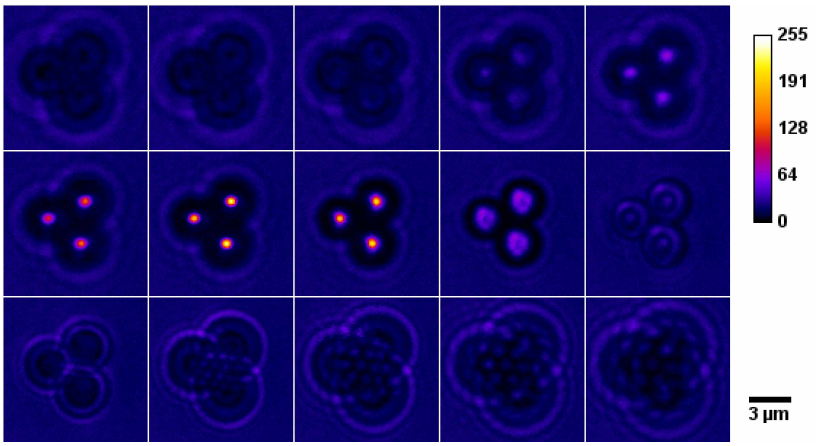

Fig. 10. Same as Fig. 2 for a group of 3 spheres of 3 μm diameter. Note that in this particular case, the detection plane moves towards the spheres by steps of 1 μm between each 2D scan.

comes within the framework of photonic molecules [7]. Raw data obtained for a group of three spheres of diameter 3 μm in contact are shown in Fig. 10. It appears here that the nanojet is produced independently below each sphere, without any visible coupling between spheres. Data analysis, not reported here, show that the three obtained nanojets can be characterized by the same parameters as the jet obtained on the single 3 μm sphere of Fig. 5. This observation confirms the absence of interaction for nanojets produced by plane wave excitation out of gallery

#91087 - $15.00 USD Received 20 Dec 2007; revised 31 Jan 2008; accepted 31 Jan 2008; published 1 May 2008

mode resonance. This constitutes a significant added value that is widely exploited for surfaces nanopatterning [12, 13].

5. Conclusion

Photonic nanojet have been experimentally observed using a fast scanning confocal system. Different diameters of spheres with diameter ranging from 1 up to 5 μm, deposited on a glass substrate have been investigated. Comparison with theoretical calculation show a relative good qualitative agreement. Groups of spheres in contact have been also investigated and showed that each sphere produce independently its nanojet, with negligible influence of the neighborhood. Our measurements show that photonic nanojets can be efficiently imaged by a conventional confocal microscopy system. The procedure described here can be straightforwardly extended to rapidly characterize a broad range of micro- and nanostructures.

Acknowledgments

The authors acknowledge stimulating discussions with Philippe Delaporte, Cyril Favard and Davy Gérard. This work has been funded by the grant PEPS "NANODRILL" of the Centre National de la Recherche Scientifique and by the French Agence Nationale de la Recherche under contract No. ANR-05-BLAN-0337-02.

#91087 - $15.00 USD Received 20 Dec 2007; revised 31 Jan 2008; accepted 31 Jan 2008; published 1 May 2008